Emulating Synchrophasor Frequency Measurements with Transient Stability Simulation

Zhen Dai, *Member, IEEE,* and Joseph Euzebe Tate, *Member, IEEE*

***Abstract*—In transient stability simulators such as PSS/E, the bus frequency is estimated using a window of (positive-sequence) phasor angle measurements. A digital filter is often used to account for the filtering effect in actual measurement devices and to eliminate sudden changes during frequency computations. Although transient stability simulators label the filtered angle derivative as the "frequency", the frequency provided by such programs does not match actual measurements reported by phasor measurement units (PMUs), which makes it difficult to gauge the validity of studies (e.g., wide-area event detection and control applications) that are based on such simulations. In this paper, we implement a frequency computation method directly using positive phasor angles provided by simulators. The proposed method is tested on two systems extensively and validated against the measurements of an actual PMU. The improved frequency measurements closely match PMU responses. Cross-validation results also suggest the method may be used for other systems without conducting full time-domain simulations.**

***Index Terms*—Frequency estimation, phasor measurement units, power system transient stability, power system simulation.**

I. Introduction

Frequency measurements are vital to studies such as inertia estimation [1], event detection [2], [3] and wide area controls [4]–[7]. During transients, frequency does not have an obvious meaning since voltage and current waveforms are not pure sinusoids [8]. Although phasors (and by extension frequency) are not properly defined, a quantity can still be defined to reflect the concept of frequency during transients, while it also reflects the true frequency if the system is in steady state. One common definition of bus frequency is the time derivative of voltage angle [9], which is used both in measurement devices (e.g., PMUs [10]) and transient stability simulators (e.g., PSS/E). However, there are multiple methods to approximate the derivative based on angle measurements [11]. Furthermore, the frequency computation process is often accompanied by filtering, which further impacts transient responses. For example, in PMUs, several stages of downsampling and filtering are involved before a final frequency is reported [12]. Additional signal processing steps (e.g., ignoring phase jumps [13]) has also been suggested for synchrophasor calculations during transients. By contrast, bus frequency reported by transient stability simulators is often calculated by a much simpler algorithm (e.g., a low pass filter and a washout filter [11]) over which the users have little control.

Z. Dai and J. Tate are with the Department of Electrical and Computer Engineering, University of Toronto, Toronto, ON, Canada e-mail: daizhen07@gmail.com. This work was supported by the Natural Sciences and Engineering Research Council of Canada (NSERC) under Discovery Grant NSERC RGPIN-2016-06674.

With an increasing number of PMUs installed, great efforts have been made to develop wide-area monitoring and control applications to exploit their synchronized data. In order to fully test responses of a PMU, time-domain waveforms are needed, which are often provided by electromagnetic transients (EMT) programs where detailed models are required. Although the EMT-type simulation can be used for prototyping [7], it is computationally expensive and often relies on dedicated hardware [14] [15], particularly for large-scale power systems. In addition, full EMT models are usually not available for interconnected systems (e.g., the Eastern Interconnection). Furthermore, for PMU-based studies, since the reporting rate of PMUs is relatively low (i.e., several samples per cycle) compared to electromagnetic transients, depending on the type of applications, it is possible that full EMT simulation is not necessary [11]. As a result, testing and prototyping of PMU-based applications (e.g., [6]) still heavily rely on transient stability (TS) simulations despite the reduced time resolution and modeling capability (see [16] for a more comprehensive discussion of differences between the two types of simulators). It is necessary for researchers to be aware of the potential discrepancy between the frequency that would be reported in the field (as measured by PMUs, given time-domain waveforms) and simulated frequency (filtered in TS programs). This discrepancy is largely unaccounted for in previous studies and makes it difficult to gauge the performance of PMU-based applications based on TS simulations. Instead of relying on already-filtered bus frequencies provided by the TS programs, our research goal is to emulate realistic frequency signals based on unfiltered phase angles, which ultimately would facilitate prototyping PMU-based applications.

In this paper, we propose a frequency computation method using (positive sequence) voltage phasor angles in PSS/E, which is tested against recorded PMU measurements from an SEL 451 [12] on both the IEEE 9-bus and the 39-bus systems. In addition to the main frequency computation algorithm (phase angle differencing and truncated mean filter), the method also includes two extra steps: *a)* pre-event (steady-state) angle compensation and low pass filtering, and *b)* post-processing frequency filtering using an ARX model [17] to further improve accuracy. The results demonstrate that the resulting frequency measurements match actual PMU measurements closely with little computational costs. Although we mainly focus on generator outage events, the proposed framework can be applied to other events (e.g., bus faults) to improve frequency measurements. However, the optimal parameters of the post-processing frequency filter (i.e., the ARX model) are dependent on the event type. In summary,

the main contributions and results include:

1) The results clearly demonstrate, compared to the default filtered frequency measurements output from the TS simulator, the proposed models offer significant improvements.
2) The post-processing step can be used to further improve accuracy. Based on cross-validation, the parameters are within a small range, which can be potentially used for a different system with similar events.

The rest of the paper is structured as follows. In Section II, we first review the basic components of frequency calculation using phasor measurement units. The two test systems that experience frequency disturbances due to generator tripping or 3-phase bus faults are introduced in Section III along with the hardware setup. Section IV provides comprehensive frequency results obtained from various methods. Multiple comparisons are conducted to evaluate the proposed method. Concluding remarks are presented in Section V. The appendices include demonstrations of the truncated mean filter (Appendix A) and the effect of angle compensation and LPF (Appendix B).

II. Synchronized Frequency Computation

Fig. 1 illustrates the frequency computation processes of an actual PMU ($f_{\mathcal{P}}$) and the proposed method (PSS/E-vPMU+, labeled as $f_{\mathcal{V}_+}$) based on PSS/E simulation. In an actual PMU, three-phase voltage waveforms are processed to produce positive sequence phasors in order to compute frequency and RoCoF following steps 0-4 and 6. In our experimental setup, PSCAD/EMTDC was used to generate three-phase waveforms (labeled as Vabc in Fig. 1) which were then "played back" into a PMU (SEL 451).

For transient stability simulators, only positive sequence phasors are available for frequency computation. As a result, we mainly focus on the steps from 4 onward. Based on different steps involved, several virtual PMU models were built. To demonstrate the effect of angle compensation and filtering, a simple model PSS/E-vPMU- (step 4 and 6, labeled $f_{\mathcal{V}_-}$) is first discussed. PSS/E-vPMU (labeled $f_{\mathcal{V}}$) represents the frequency computation process based on steps 4-6. However, the intermediate frequency results after step 6 might be different from the results given by PMUs, and an extra filter (step 7) is introduced to further improve accuracy, and thus yields the final proposed frequency computation method, PSS/E-vPMU+ ($f_{\mathcal{V}_+}$). By contrast, the frequency directly reported from PSS/E ($f_{\mathcal{D}}$) is calculated by an unspecified algorithm and filtering technique.

In summary, Table I shows the notations for different frequency measurements to be discussed in subsequent sections. The PMU and PSS/E-default frequency serve as benchmarks for comparison, while the remaining three represent intermediate and final versions of the proposed method. Although practical implementations are proprietary and may vary depending on manufacturers, the IEEE standard [10] provides example algorithms for the two measurement classes P and M, which will not be discussed here. Algorithms used in this paper are presented as follows except the angle compensation (which is demonstrated in the case study section IV-C).

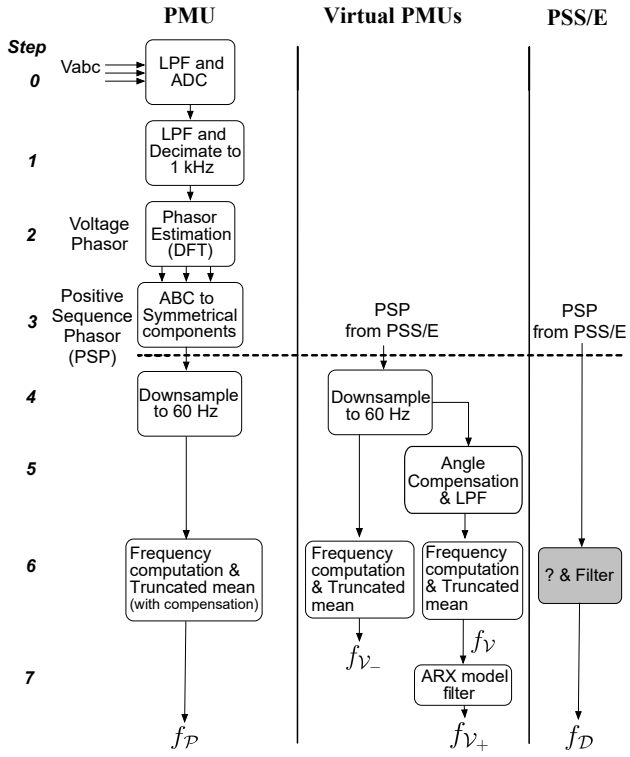

Fig. 1. Synchrophasor computation block diagram. Frequencies of various candidates are labeled as f_i, $i \in \{\mathcal{P}, \mathcal{D}, \mathcal{V}, \mathcal{V}-, \mathcal{V}+\}$. (LPF stands for low-pass filter. ADC is analog-to-digital converter.)

TABLE I
Frequency Computation Methods

Method	Notation	Steps involved[1]	Notes
PMU	$\mathcal{P}$	0-4 and 6	benchmark
PSS/E-vPMU-	$\mathcal{V}_-$	4 and 5	without compensation
PSS/E-vPMU	$\mathcal{V}$	4, 5 and 6	proposed input
PSS/E-vPMU+	$\mathcal{V}_+$	4-7	proposed frequency
PSS/E-default	$\mathcal{D}$	N/A	benchmark

A. Filters (Steps 0, 1, 4-6)

There are three filters in an SEL 451: an analog filter and two digital filters corresponding to step 0, 1 and 4, respectively. Based on the manual of SEL 451 [12], the following parameters are specified for the following filters:

- The filter at step 0 has a cutoff frequency of 3 kHz, which is less than half the sampling frequency (8 kHz).
- The half-power (-3 dB) point for the second filter (at step 1) is 250 Hz when downsampled to 1 kHz.
- A digital filter (defined by frequency responses at step 4) is used before downsampling to 60 Hz (i.e., the reporting as well as the nominal frequency, denoted by f_0).
- A truncated mean filter (at step 6) is applied to the calculated frequency measurements before they are reported.

In spite of the specifications, it is left unspecified what type or order of filters are used in the relay. According to [18], for most practical purposes a simple averaging filter (the so-called box-car filter) is sufficiently accurate. However, studies of PMU performances for specific PMU applications may require detailed filtering models (e.g., [4]).

[1]The step numbers are defined in Fig. 1.

Similar processes can be reproduced during simulation given three-phase time series measurements of the voltage (e.g., as produced in PSCAD or Simscape). In transient stability programs, however, simple digital filters are used, which can not fully represent the responses of actual PMUs. To mimic the effect of low-pass filtering in an actual PMU, we use a low-pass filter (Butterworth, 5th order) with a cut-off frequency of 15 Hz at step 5. Details about filter implementation are discussed further in the case study section IV-C.

B. Downsampling (Steps 1 and 4)

Downsampling happens at step 1 and 4 in Fig. 1. It is achieved internally in a PMU. In PSS/E, the default solution time step is 8.333 ms (2 samples per cycle). Simple downsampling (sometimes referred to as decimating) is accomplished by a 1/N resampling (i.e., taking every Nth sample). The PSS/E measurements are downsampled to 60 Hz to compare with the actual PMU.

C. Frequency Computation (Step 6)

1) Synchrophasor frequency: For SEL 451 relays, the frequency at time t ($f[t]$) is determined by the positive sequence phase angle $\theta[t]$ and $\theta[t-1]$ (in radians).

$$f[t] = \frac{\theta[t] - \theta[t-1]}{2\pi\Delta t} \tag{1}$$

Although the initial ADC sampling rate of the device is 8 kHz, frequency is only updated every cycle (i.e. $\Delta t = 1/f_0$) due to downsampling.

2) Truncated mean filter: Additionally, an average is calculated using a sliding window of frequency samples with a window length that is dependent on the PMU setting. For the "smooth" application setting, the average is calculated as follows:

$$\bar{f}[t] = \frac{\sum_{j=0}^{9} f[t-j] - f_{max1} - f_{max2} - f_{min1} - f_{min2}}{6}, \tag{2}$$

where f_{max1} and f_{max2} are the two largest frequency deviations in the last 10 samples. Namely, $f_{max1} \geq f_{max2} \geq \forall f_j$ and $f_{max1}, f_{max2} \in \{f_j | j = t-9, t-8, \ldots, t\}$. Similarly, f_{min1}, f_{min2} are the two smallest frequency deviations. A theoretical analysis of generalized truncated mean filter (alpha-trimmed mean filter) is provided in [19]. The rate of change of frequency is also updated every cycle using the averaged frequencies deviations.

$$RoCoF_t = \frac{\bar{f}[t] - \bar{f}[t-1]}{\Delta t} \tag{3}$$

The measured frequency is computed as $\bar{f}[t] + f_0$ (when the frequency deviation is within band as defined in [12]). However, since PSS/E reports per unit frequency deviation, all PMU frequency measurements are converted properly for comparison.

D. Post-processing of Frequency (Step 7)

In order to better match the frequency computed based on transient stability simulations to PMU measurements, an extra processing step can be implemented. Multiple model structures can be chosen to accomplish this goal. The autoregressive exogenous (ARX) model [17] [20] is widely used for its simplicity and its ability to incorporate exogenous inputs. Evaluation and system identification of ARX models are also readily available in popular scientific computation tools such as MATLAB [21] and R [22].

By definition, the ARX structure is

$$\begin{aligned} y[t] = &- a_1 y[t-1] - \ldots - a_n y[t-n] \\ &+ b_1 u[t] + \ldots + b_m u[t-m+1] + e[t] \end{aligned} \tag{4}$$

where u, y and e are the input, output and error respectively. An ARX model can be identified given the input $f_{\mathcal{V}}$ (i.e., PSS/E-vPMU output) and the output $f_{\mathcal{P}}$ (i.e., recorded PMU output). The estimated output given by the ARX is $f_{\mathcal{V}_+}$ which should match the output $f_{\mathcal{P}}$ closely. Note that the simulated and recorded frequency measurements from different sources are aligned based on the initial deviation from the steady-state behavior thus eliminating delay. If latency can be measured reliably, then during the identification process, the delay should be first identified and then eliminated, and the same computation framework can be followed. Further details about time alignment are presented in Section III-C.

The number of unknown coefficients (the order of each polynomials n and m) can be determined based on various criteria [17]. In general, higher order models yield lower estimation error, especially when the models are evaluated using the same data set for both identification and validation. The use of higher order models, however, may lead to over-fitting and marginally higher computation costs. We considered all m and n where $n \leq 5$ and $m \leq 5$ in (4). The model that yields the highest goodness of fit value (defined in (5) and (6) with $\mathcal{S}$ consisting of all scenarios) is when $m = 1$ and $n = 2$ for both test systems, which is selected as the ARX model order for the case study.

III. Test Systems

To evaluate the frequency computation methods and ensure a fair comparison, the same test systems are implemented. The IEEE 9-bus system and the 39-bus (also known as the New England system) are built in both PSS/E and PSCAD/EMTDC. The dynamic models of the New England system are provided in [23]–[25]; details for the 9-bus system are provided in [8], [26]. We first present the simulation setup then the relay setup.

A. Simulation

The simulation time step for PSCAD is 20 μs, while for PSS/E, it is 8.333 ms ($\approx 1/120$ Hz). Great efforts have been made to match the power flows ([27], [28]) and dynamic models in both platforms. In spite of model differences (e.g., the Bergeron model versus the π model) in PSCAD and PSS/E, after proper initialization of machine controls, the differences between the two simulators are very small. For example, for the IEEE 39-bus system, the average active generation error

between the two platforms is 0.3%, the average generator terminal voltage magnitude error is 0.11%, and the average phase angle error is 0.09%. In addition to the 10 generator buses (30 to 39), PMUs are also placed at buses 1, 3, 9, 12, 16, 19, and 28. The mean voltage magnitude error of these buses is 0.16%. For the 9 bus system, PMUs are assumed to be installed at all buses. Measurements at PMU buses are collected when outages of non-equivalent generators are introduced in both systems. Namely, generators at buses 31 to 39 of the 39-bus system and at buses 2 and 3 of the 9-bus system are outaged.

B. Relay Test System

In order to compare simulation results and sychrophasor measurements from an actual PMU, the following setup and protocols were used:

1) Export 3-phase voltage waveforms in COMTRADE format [29] from PSCAD.
2) Import COMTRADE data into the compactRIO (cRIO) platform for digital-to-analog conversion [30].
3) Connect the cRIO to the low-energy testing module of the SEL 451.
4) Monitor and archive PMU outputs using the phasor data concentrator software OpenECA [31].
5) Export archived data from SQL server to MATLAB and perform analysis.

Note that the choice of specific hardware and software tools (e.g., cRIO, OpenECA), data format (e.g., COMTRADE) and sampling rate (e.g., 154 kHz for the cRIO) can be replaced or modified as long as the generated signals can faithfully represent system responses with a sampling rate higher or equal to the PMU ADC sampling rate (8 kHz in our case).

C. Time alignment

The synchrophasor outputs from PMUs are time stamped using the GPS system. Although the synchronized data are based on simulation results in PSCAD, the corresponding event time in UTC time can not be determined easily even with transfer latency excluded. This is because PMUs do not provide time-stamped three-phase input waveforms directly. The event time is unclear given only time-stamped phasor measurements due to the delay and/or distortion introduced by filtering and phasor estimation. Additionally, the sampling rate and reporting rate used by different devices may vary. To avoid ambiguity and uncertainty, frequency measurements from different platforms are aligned such that the last steady-state samples coincide by applying thresholds on the frequency and RoCoF measurements. This corresponds to the case where all input delays (possibly including filtering and estimation group delay) are compensated.

IV. Case study

Outages of various generators are introduced in both test systems, since this tends to result in significant frequency responses (versus other types of outages). According to [9], there are four stages after disturbances involving generation-load mismatch. We focus on the first two stages (from 0 to 2 seconds after disturbance), where generator outputs are determined first by network impedance and then by inertia. During this period, large angle changes are expected followed by rapid declines of rotor speeds, which are widely used for event detection and frequency response related studies, where the largest RoCoF in absolute value is of interest. To gauge the generalization of the proposed model to different types of events, 3-phase-to-ground bus faults were also simulated for the 9-bus system.

A. Methodology

Our goal is to develop a frequency computation method that can be directly applied to phase angle output from a transient stability simulator so that the resulting frequency measurements match what an actual PMU would report. To quantify the differences between various frequency sources, the following measure (referred to as the goodness of fit hereafter) based on the normalized root-mean-square error is used:

$$F_i^{(s)} = 1 - \frac{\|\boldsymbol{f}_{\mathcal{P}}^{(s)} - \boldsymbol{f}_i^{(s)}\|}{\|\boldsymbol{f}_{\mathcal{P}}^{(s)} - 1/N \sum_{t=1}^{N} f_{\mathcal{P}}^{(s)}[t]\|}. \tag{5}$$

$\boldsymbol{f}_i^{(s)}$ represents a frequency vector (i.e., a time series observed given scenario s), where $i \in \{\mathcal{D}, \mathcal{V}_-, \mathcal{V}, \mathcal{V}_+\}$ (in Table I). Note that unless otherwise stated, the PMU measurement $\boldsymbol{f}_{\mathcal{P}}$ is used as the reference to compute the goodness of fit F_i. In order to better evaluate the performance of the proposed method, an average of $F_i^{(s)}$ over different scenarios is used. For example, the average goodness of fit of a set of scenarios (defined by $\mathcal{S}$) is calculated as follows:

$$\bar{F}_i^{(\mathcal{S})} = \frac{1}{\|\mathcal{S}\|} \sum_{s \in \mathcal{S}} F_i^{(s)}, \tag{6}$$

where $\|\mathcal{S}\|$ denotes the cardinality of the set $\mathcal{S}$. In practice, $\mathcal{S}$ may represent any subset of the available scenarios (e.g., observations at various PMUs based on various events being randomly and repeatedly split into two sets—one for training and one for validation).

To capture frequency responses within the first two stages of a generation-load mismatch, in all case studies, the goodness of fit in (5) is calculated using a window size of $N = 138$ (i.e., 2.3 s), while $t = 1$ corresponds to the first sample that deviates from the steady-state frequency. The results of various methods are presented below first through example frequency measurement plots then using statistical summaries. In addition to evaluation of the proposed frequency computation methods on each of the systems, a cross evaluation of ARX model parameters is also included.

B. Motivation: $f_{\mathcal{P}}$ vs $f_{\mathcal{D}}$

Before we move onto the proposed method, it is important to ensure the systems used by PSCAD and PSS/E are the same so that subsequent comparisons based on the two are fair. Rotor speeds are available in both simulators and directly comparable

without any filters. Despite our best efforts in matching the PSS/E and PSCAD simulations, there is a slight discrepancy (0.00013 pu) between the two frequencies in the pre-outage steady-state, which is compensated for in Fig. 2 and 3 by adding a constant offset of 0.00013 pu to the PSCAD-based rotor speed and frequency signals. This offset also results in a discrepancy in the phasor angles reported by PSS/E and PSCAD, which is addressed via the angle compensation technique described in Section IV-C and Appendix B. Fig. 2 and Fig. 3 show the comparison of frequencies from various sources at bus 33 when generator 3 (located at bus 32) is tripped in the 39-bus system. The rotor speeds decrease smoothly prior to all frequencies. The discrepancy between the two provides a measure of how similar the dynamic models are. Based on a $\bar{F}$ value of about 0.93 (evaluated using rotor speed, instead of frequency, with the reference being the PSCAD rotor speed) and the power flow differences in Section III, we conclude that the test systems in two simulators are close enough to be considered as the same.

First, the comparison of PMU measurement $f_{\mathcal{P}}$ and PSS/E default frequency $f_{\mathcal{D}}$ is presented. Clearly, in Fig. 2 and 3, the PSS/E frequency $f_{\mathcal{D}}$ (in dashed line) deviates from the PMU measurement (in red). Particularly, during the transients

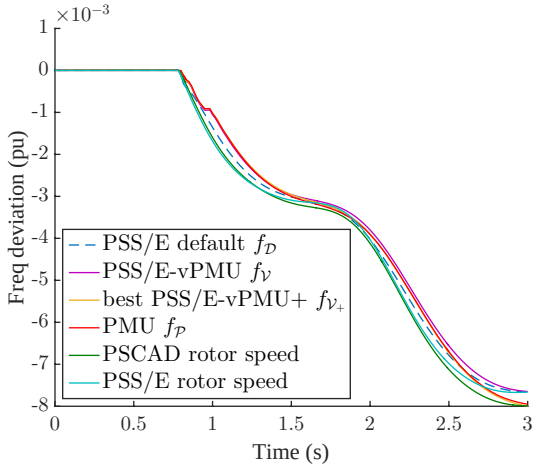

Fig. 2. Comparison of frequency and rotor speed results (at bus 33 when the generator at bus 32 is outaged).

(starting from 0.8 s to around 1.4 s in Fig. 3), the PMU frequency shows significant delays and distortions compared to the PSS/E one as well as to the smooth rotor speeds. These results provide a clear motivation for developing alternative frequency computation methods. Note that there is a plateau around 0.95 s in both recorded and simulated PMU frequencies, which is the result of the truncated mean in (2) (see Appendix A for more information).

An extreme case would be when the PMU is located at the terminal of the outaged generator. From Fig. 4, we can see the distortion of the PMU measurement at the outage location is much worse compared to Fig. 3 with a large valley between 0.8 to 0.95 s. In contrast, the PSS/E measurement is still similar to that in Fig. 3. In summary, this indicates the bus frequency signal model with a single user-defined filter constant (0.0333 by default) in PSS/E is not sufficient to capture the complex response of an actual PMU. By comparison, the proposed

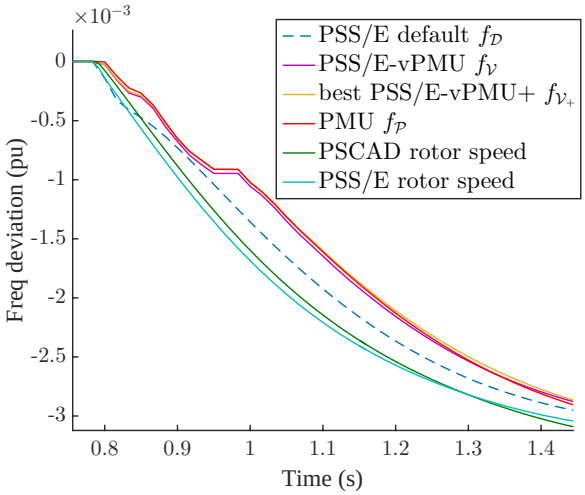

Fig. 3. Comparison of frequency results (at bus 33 when the generator at bus 32 is outaged).

vPMU models show significant improvements (see the yellow and purple lines in all three figures), which will be discussed next.

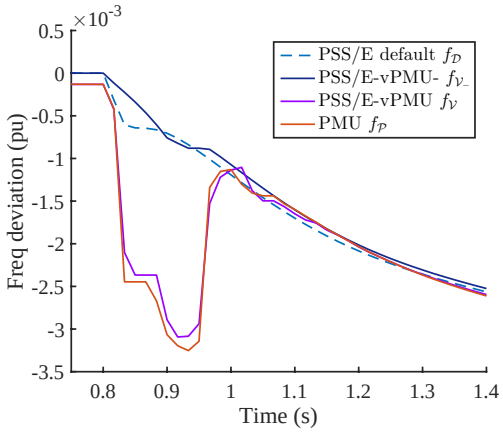

Fig. 4. Comparison of frequency results (at bus 32 when the generator at bus 32 is outaged). The steady-state frequency deviation of 0.00013 pu between PSCAD and PSS/E, which is compensated for in Figures 2 and 3, is explicitly shown in this figure to illustrate the impact of angle compensation.

C. Effects of angle compensation and LPF: $f_{\mathcal{V}_-}$ vs $f_{\mathcal{V}}$

Fig. 4 also shows the steady state frequency deviation (about -0.00013 pu, simulated in PSCAD and measured by PMU), which corresponds to a decreasing phasor angle during steady state (see Fig. 11 in the Appendix B). In general, it does not cause inaccurate frequency results, since only the angle difference is used, and the effect may be compensated using manufacturer-dependent compensation algorithms. However, during transients, phasor angles may change significantly (e.g., due to generators or line outages). For example, the corresponding angle drop is about 18 degrees in Fig. 4 within the first 5 samples after the tripping, while it is about 2 degrees in Fig. 3. The combined effects of filtering and angle jump become salient in actual PMUs, which can not be ignored. Meanwhile, in PSS/E, the angle jumps happen instantaneously. To account for the impact of frequency deviation on angle, the

following equation is used for updating the phase angle for the tth sample:

$$\theta_{\mathcal{V}}[t] = \theta_{\mathcal{V}_-}[t] + 2\pi t \Delta t (f_{\mathcal{P}_s} - f_0) + \theta_{\mathcal{P}}[1] - \theta_{\mathcal{V}_-}[1]. \quad (7)$$

The subscripts indicate the source of measurements. Namely, the PSS/E simulated angles $\theta_{\mathcal{V}_-}[t]$ (after step 4) are compensated with an incremental angle calculated using the steady state frequency deviation (in Hz) recorded by the PMU ($f_{\mathcal{P}_s} - f_0$). The new angle $\theta_{\mathcal{V}}$ is then used in (1) to compute the frequency $f_{\mathcal{V}}$. Note that the offset $\theta_{\mathcal{P}}[1] - \theta_{\mathcal{V}_-}[1]$ does not impact dynamic behaviors, but it is used to allow a direct comparison of angles between simulation and recorded PMU measurements. Without angle compensation in (7) or filtering, the frequency calculated using $\theta_{\mathcal{V}_-}$ (i.e., $f_{\mathcal{V}_-}$, the red line labeled as PSSE-vPMU- in Fig. 4) is very smooth compared to the actual PMU results, since the "valley" does not appear. In contrast, when the effect is accounted for, the PSS/E-vPMU matches the actual PMU closely by recreating the frequency deviation and valley. Note that the choice of low pass filter would impact the dynamic responses (e.g., the shape of the valley). Based on the goodness of fit of phase angles in the 39-bus system, a 5th order Butterworth filter is used in this study (see visual examples in Fig. 11).

In summary, the proposed angle compensation with filtering should be used if transient responses are of concern. From now on, all inputs used for the ARX models are properly compensated. Namely, PSS/E-vPMU ($f_{\mathcal{V}}$) is used as the inputs for the ARX models.

D. Effect of the ARX model: $f_{\mathcal{V}_+}$

As Table II shows, the average goodness of fit values between PSS/E default and the actual PMU ($\bar{F}_{\mathcal{D}}$) is only 91.63% and 93.37% for the 39 bus and 9 bus system, respectively. Previous figures also show promising results of the proposed PSS/E-vPMU. However, as an alternative, although PSS/E-vPMU performs better than the direct measurement from PSS/E ($\bar{F}_{\mathcal{V}} = 93.05\%$ for the 39-bus system, and 95.56% for the 9-bus system), it still deviates from the PMU results. An extra post-filtering step (defined by an ARX model) is introduced to further improve the model accuracy. In order to estimate the parameters of the ARX model and prevent over-fitting, all observations (considering all outages and PMU locations) of each test system are divided into different subsets based on k-fold cross-validation [21], where $k = 10$ for the 39-bus system and 5 for the 9-bus system. From Table II, we can see that, on average (across all folds), the ARX model can further improve accuracy as indicated by an $\bar{F}_{\mathcal{V}_+}$ of more than 97.3% for both systems. Later, among all folds, the best PSS/E-vPMU+ model is selected based on the highest $\bar{F}_{\mathcal{V}_+}$ of the testing set. Visualization of summary statistics are presented next.

TABLE II
GOODNESS OF FIT COMPARISON OF TWO SYSTEMS (OUTAGES)

Measure	$\bar{F}_{\mathcal{D}}$	$\bar{F}_{\mathcal{V}}$	$\bar{F}_{\mathcal{V}_+}$ training	$\bar{F}_{\mathcal{V}_+}$ testing	$\bar{F}_{\mathcal{V}_+}$ total
39 bus	91.63%	93.05%	97.71%	97.70%	97.71%
9 bus	93.37%	95.56%	97.33%	97.32%	97.33%

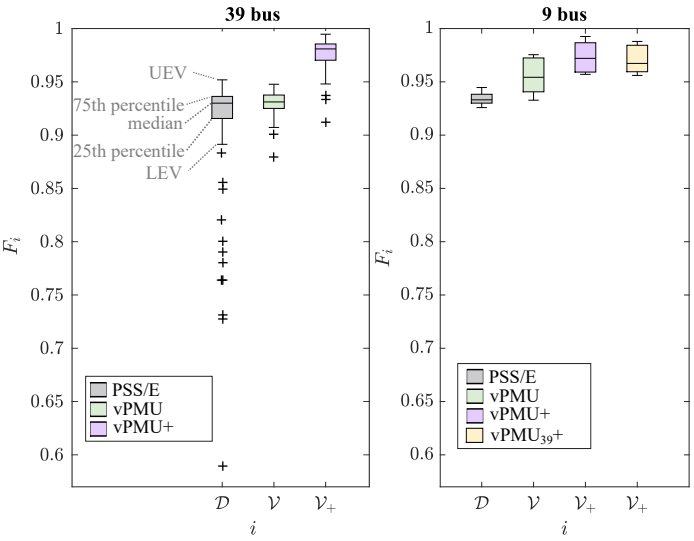

Fig. 5. Box plots of the goodness-of-fit values of various methods for the 39-bus system (left) and the 9-bus system (right).

Fig. 5 shows the box plots of the goodness-of-fit values when various methods are used, which provide visual comparison of variability. The standard box plot definition (see legends in Fig. 5) in [32] is used, where UEV and LEV represent the upper and lower extreme values, respectively. UEV $= Q3 + 1.5(Q3 - Q1)$ and LEV $= Q1 - 1.5(Q3 - Q1)$, where $Q1$ and $Q3$ correspond to the 25th and 75th quantile, and $(Q3 - Q1)$ is the interquartile range (IQR). Samples that are outside of the extreme values are considered as outliers (labeled as $+$). Both IQR and extreme values (sometimes also known as inner and outer fences) show how spread the data is. The grey box (labeled PSS/E and $i = \mathcal{D}$) represents the quantile distribution of $F_{\mathcal{D}}$, and the green box (labeled vPMU and $i = \mathcal{V}$) represents the quantiles of $F_{\mathcal{V}}$.

For the 39-bus system (in the left subplot), the number of outliers (i.e., mostly cases with large angle changes immediately after the outage), IQR, as well as the median value indicate the default PSS/E frequency is a poor representation of actual PMU measurements. For example, the worst $F_{\mathcal{D}}$ (i.e., the lowest outlier) is only 59%. By comparison, the proposed PSS/E-vPMU significantly decreases the number of outliers and provides tighter IQR with a higher average F value even without the post-filtering ARX model applied. Specifically, the variance of $F_{\mathcal{D}}$ is 0.0022, while the variance of $F_{\mathcal{V}}$ is reduced to less than 0.0001. This is desirable since it indicates the proposed method was able to improve the frequency measurement accuracy with fewer extreme errors. This also suggests that accuracy of the proposed frequency computation methods are less dependent on specific scenarios (e.g., location of outages and PMUs). The purple box is based on results given by the best PSS/E-vPMU+ method (referred to later in the 9-bus case evaluations as PSS/E-vPMU$_{39}$+). Incorporating the ARX model leads to a significantly higher median, which indicates that the goodness of fit has been further improved. The results agree with the improvements of $\bar{F}_{\mathcal{V}_+}$ in Table II (by about 6.1% and 4.6%, compared to the PSS/E-vPMU and PSS/E default cases, respectively).

E. Best ARX model selection

The k-fold cross-validation results of the 39-bus system are presented in Fig. 6. The blue and pink boxes represent the performance of 10 ARX models based on 10 sets of training and testing data sets, respectively. The total average ($\bar{F}_{\mathcal{V}_+}$ total in Table II) is highlighted by a horizontal red line. Since the pink and blue boxes show little divergence in performance between the training and testing data, we can conclude that there is no over-fitting.

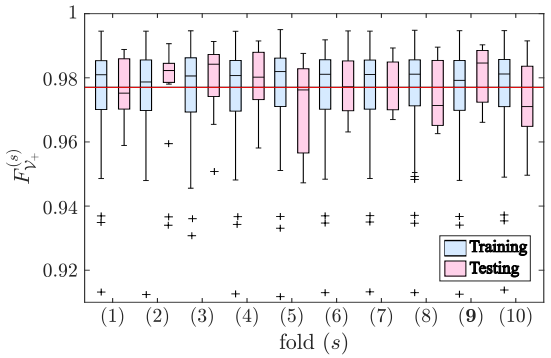

Fig. 6. Goodness of fit of various ARX models (39-bus system). The horizontal line represents $\bar{F}_{\mathcal{V}_+}$ testing. Fold (9) corresponds to the best model.

Fig. 7 visualizes the same data by explicitly assigning each measurement (for each PMU, for each outage, totaling $17 \times 9 = 153$ measurements) to a column and each model a row. The lighter color of $F_{\mathcal{V}}$ and even lighter $F_{\mathcal{V}_+}$ indicate that the proposed methods are able to increase the overall goodness of fit. In particular, for cases that are previously identified as outliers (very dark elements in the first row) when comparing PSS/E frequency measurements to PMU measurements, the proposed methods show significant improvements. This corresponds to the reduction in outliers in $F_{\mathcal{V}}$ and $F_{\mathcal{V}_+}$ in Fig. 5. Additionally, the minimal difference in $F_{\mathcal{V}_+}$ between the best and worst models (i.e., models with the highest and lowest $\bar{F}_{\mathcal{V}_+}$ of the testing set, respectively) again demonstrates that there is no over-fitting, since the performance of models does not vary given different measurements.

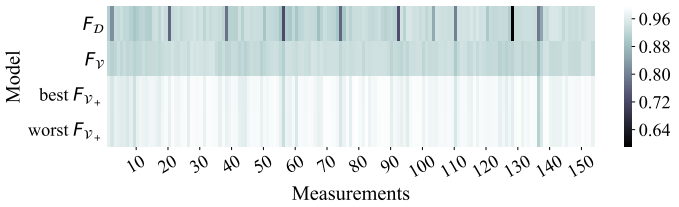

Fig. 7. Goodness of fit of various ARX models (the 39-bus system)

The box plots of the F values for the 9-bus system are presented in the right subplot of Fig. 5. We notice that the PSS/E default ($F_{\mathcal{D}}$) fit is generally better, with fewer outliers, compared to the 39-bus system. This is because the system is less diverse, since it is a much smaller system with a large equivalent generator at bus 1 (with an inertia constant of 23.64). The outages of generator 2 and 3 will lead to smaller angle changes as well as frequency declines. Similar to the 39-bus system, the results show improvements when the ARX models are used and there is no indication of over-fitting.

To prove that the ARX models can be potentially used by another system, we used the best model from the 39-bus system on observations from the 9-bus system. The resulting $F_{\mathcal{V}+}$ is represented by the yellow box plot (labeled vPMU$_{39}$+) in Fig. 5. The performance is similar to that of the best model (the purple box, labeled vPMU+) directly trained using the 9-bus system observations with slightly lower median. Specifically, when using the best model from the 39-bus system, $\bar{F}_{\mathcal{V}_+} = 97.01\%$ and is about 0.3% lower than the best model directly trained on the 9-bus system data.

Meanwhile, Fig. 8 provides the box plots of the three ARX model parameters for both test systems. Based on the medians, the parameters are very similar with little variability (based on tight IQR and extreme values). The parameters of the best ARX models for the two systems are also close (see the first two rows of Table III), which again explains the similar performances in Fig. 5 when comparing the purple and yellow boxes (vPMU+, vPMU$_{39}$+).

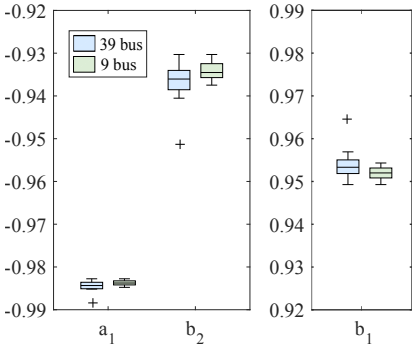

Fig. 8. Box plot of ARX parameters

TABLE III
PARAMETERS OF THE BEST ARX MODELS

a_1	b_1	b_2	Model training set
-0.9848	0.9543	-0.9375	39-bus outages
-0.9836	0.9516	-0.9335	9-bus outages
-0.9858	1.0239	-1.0122	9-bus faults

F. Other events: 3-phase bus faults

The frequency computation methods have been proposed and tested for generator outage events. To investigate the effectiveness of the methods under different conditions, more experiments were conducted by applying 3-phase-to-ground bus faults at bus 4, 5, and 6 in the 9-bus system. The same framework and evaluation process were followed. Note that to ensure a fair comparison, the logic used by SEL 451 to hold frequency output as constant when the frequency exceeds ± 20 Hz or voltage magnitude is lower than 0.1 nominal voltage is implemented for all PSS/E-based frequency methods (including default PSS/E frequency).

First, the left subplot of Fig. 9 shows the box plots of F values if bus fault cases are considered, i.e., $\mathcal{S}$ consists of bus fault scenarios in (6). Compared to Fig. 5, the default PSS/E frequency (grey box) performs badly with a mean around 77.07% and median around 71.56%. The proposed vPMU (green box) significantly improves the accuracy as $\bar{F}_{\mathcal{V}} = 87.13\%$. The purple box shows a further improvement

on the goodness of fit about 3% ($\bar{F}_{\mathcal{V}_+} = 90.44\%$) when the best ARX model is used, which is based on the 5-fold cross-validation results of bus fault cases. The overall goodness of

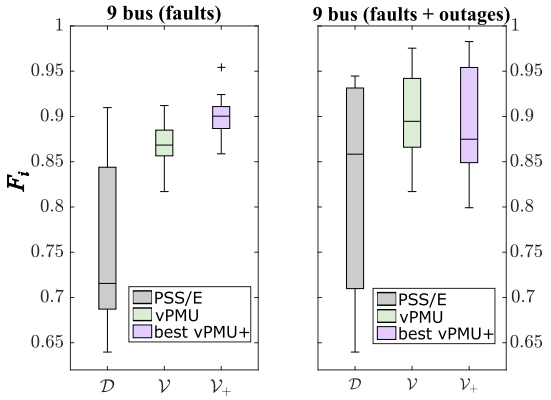

Fig. 9. Box plots of the goodness-of-fit values of various methods applied to fault cases (left) and all fault and outage cases (right) in the 9-bus system.

fit is lower than the generator outage cases since much more complicated and less homogeneous transient responses across the system are introduced due to bus faults. The parameters are also different from the previous ones (see the second and third rows in Table III). This suggests the best model under one type of events may not be optimal under another.

In order to find a universal model, all cases (i.e., $\mathcal{S}$ consisting of both faults and outages) are combined into a single event set, the results are presented in the right plot of Fig. 9. We can see that the vPMU still performs significantly better than the default PSS/E frequency measurements. However, with a lower median of F, the vPMU+ does not always lead to better performance. Considering the vPMU+ performs well when only one type of event is trained and simulated (see all the other purple boxes in Fig. 5 and Fig. 9), there is clearly a trade-off between a generic model and accuracy. Further experimental results showed that increasing the model order naively would not help (e.g., with $n_a = n_b = 5$, the median is still 2% lower than vPMU).

A further attempt at a generic model was conducted by first differencing the frequency measurements and constructing an ARIX model [20]. The ARIX models were trained using (1) only outage cases and (2) all fault and outage cases as training sets. The improvement obtained in both cases, however, was minimal (approximately 0.5% improvement in the median, compared to the vPMU). Based on the results, we suggest using specific PSS/E-vPMU+ models in Table III if the event type is known. Otherwise, the PSS/E-vPMU model may be used but with smaller improvements.

V. Conclusions

In this paper, we reviewed frequency computation methods for synchrophasors used in PMUs and transient stability software. An alternative frequency computation method is presented based on positive sequence phasor angles provided by transient stability programs so that the resulting frequency measurements better emulate those of actual PMUs. The methods have been implemented and tested using two test systems and validated against an SEL 451. Instead of using bus frequency directly given by the phasor-based transient stability simulators, we improved the accuracy of frequency through angle compensation, filtering and ARX-based post-processing. The results indicate that the proposed method is able to improve the goodness of fit by about 6% and 4% respectively for the 39 and 9 bus systems for generator outage events when compared against the default PSS/E frequencies. For bus fault events, the improvement is 13.4%. Additionally, the proposed methods significantly reduce the number of outliers suggesting overall better and much more consistent performances than the default PSS/E measurements. The ARX parameters remain relatively the same for different cases, which suggests that the PSS/E-vPMU+ model is general enough to be used with multiple systems without retraining given the same event type. This is a key advantage, since the training process requires EMTP simulation of the entire system to generate the ground truth data used in fitting the models.

In summary, our study should raise awareness of the discrepancy between actual PMUs and transient stability simulators in terms of transient frequency and angle measurements. The proposed method provides a better way to emulate frequency measurements based on angles provided by TS programs and can be potentially used for other systems. Future work may include applying the framework using various test systems, PMU models (e.g., PMUs with alternative frequency computation algorithms and filters), and simulation tools given different types of events to see if the results are consistent.

Appendix A
Truncated Mean

The truncated mean (2) of frequency is calculated and reported as the final frequency. The averaging effect may lead to undesirable results. For example, we notice that in Fig. 3 there is a plateau at around 0.95 s for PMU and PSS/E-vPMU measurements. This is due to the truncated mean filter in the PMU algorithm. Fig. 10 provides an example of frequency measurements before the truncated mean filter.

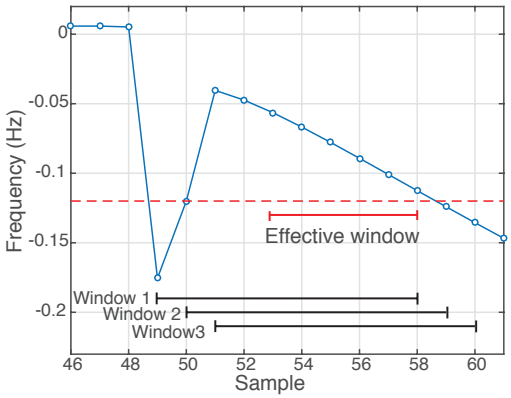

Fig. 10. Effect of truncated mean defined in (2)

The sharp decrease in frequency is due to transients of phase angles. The truncated mean is computed by averaging over a 10-sample window with 2 maximum and 2 minimum points excluded. The three windows all share the same six points for average, which leads to the same final reported

frequency, hence the plateau. Similar results may appear when other moving average filters are applied. Note that the RoCoF measurements would include the same artifacts of the truncated mean filter, since they are computed using the filtered frequency measurements (see (3)).

APPENDIX B
ANGLE COMPENSATION AND LPF

As mentioned in Section IV-C, the angle compensation and filtering are necessary to achieve a closer match to actual PMU results and avoid extreme discrepancies during transients. Fig. 11 provides examples of angles from various sources. The blue line (PSS/E comp) represents angles provided by PSS/E with compensation applied (by assuming the steady state frequency is known a prior). The actual PMU angles, however, lags the PSS/E with more dynamics as a result of multiple filters. The results demonstrate the effect of our proposed method—by applying compensation and filtering (at step 5 mentioned in Section II), the computed angle (PSS/E-vPMU) coincides much better with the actual PMU angle. In fact, the average goodness of fitness between PSS/E-vPMU and PMU angles in the 39-bus system is about 97.8%, which may be useful for other studies requiring simulated phasor angle changes.

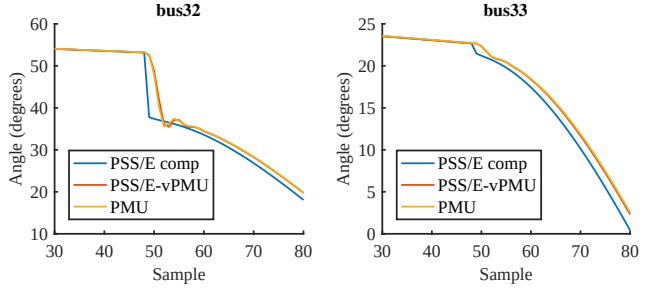

Fig. 11. The effect of angle compensation with filtering at bus 32 (left, corresponding to Fig. 4) and bus 33 (right, corresponding to Fig. 3).

REFERENCES

[1] P. Ashton, C. Saunders, G. Taylor, A. Carter, and M. Bradley, "Inertia estimation of the GB power system using synchrophasor measurements," *IEEE Transactions on Power Systems*, vol. 30, no. 2, pp. 701–709, March 2015.

[2] D. Kim, T. Y. Chun, S. Yoon, G. Lee, and Y. Shin, "Wavelet-based event detection method using PMU data," *IEEE Transactions on Smart Grid*, vol. 8, no. 3, pp. 1154–1162, May 2017.

[3] M. Cui, J. Wang, J. Tan, A. R. Florita, and Y. Zhang, "A novel event detection method using PMU data with high precision," *IEEE Transactions on Power Systems*, vol. 34, no. 1, pp. 454–466, Jan 2019.

[4] I. Kamwa, S. R. Samantaray, and G. Joos, "Compliance analysis of PMU algorithms and devices for wide-area stabilizing control of large power systems," *IEEE Transactions on Power Systems*, vol. 28, no. 2, pp. 1766–1778, May 2013.

[5] B. Hill, D. Trudnowski, and J. Wold, "Frequency estimation for the PDCI inter-area oscillation damping controller," in *2016 IEEE Power and Energy Society General Meeting (PESGM)*, July 2016, pp. 1–5.

[6] B. J. Pierre, F. Wilches-Bernal, D. A. Schoenwald, R. T. Elliott, D. J. Trudnowski, R. H. Byrne, and J. C. Neely, "Design of the pacific dc intertie wide area damping controller," *IEEE Transactions on Power Systems*, vol. 34, no. 5, pp. 3594–3604, Sep. 2019.

[7] L. Simon, K. S. Swarup, and J. Ravishankar, "Wide area oscillation damping controller for DFIG using WAMS with delay compensation," *IET Renewable Power Generation*, vol. 13, no. 1, pp. 128–137, 2019.

[8] P. W. Sauer and M. Pai, *Power system dynamics and stability*. Prentice Hall, 1998.

[9] P. Kundur, N. J. Balu, and M. G. Lauby, *Power system stability and control*. McGraw-hill New York, 1994, vol. 7.

[10] "IEEE/IEC international standard - measuring relays and protection equipment - part 118-1: Synchrophasor for power systems - measurements," *IEC/IEEE 60255-118-1:2018*, pp. 1–78, 2018.

[11] F. Milano and A. O. Manjavacas, *Frequency Variations in Power Systems: Modeling, State Estimation, and Control*, 1st ed. Wiley, Jul. 2020.

[12] *SEL-451-5 Relay Protection, Automation, and Control System Instruction Manual*, Schweitzer Engineering Laboratories, Inc., Jan 2015.

[13] A. G. Phadke and B. Kasztenny, "Synchronized phasor and frequency measurement under transient conditions," *IEEE Transactions on Power Delivery*, vol. 24, no. 1, pp. 89–95, 2009.

[14] V. Dinavahi and Y. Chen, "Multi-FPGA digital hardware design for detailed large-scale real-time electromagnetic transient simulation of power systems," *IET Generation, Transmission & Distribution*, vol. 7, no. 5, pp. 451–463, May 2013.

[15] Y. Song, Y. Chen, S. Huang, Y. Xu, Z. Yu, and J. R. Marti, "Fully GPU-based electromagnetic transient simulation considering large-scale control systems for system-level studies," *IET Generation, Transmission & Distribution*, vol. 11, no. 11, pp. 2840–2851, Aug. 2017.

[16] H. Ravindra, M. O. Faruque, M. Steurer, M. Andrus, and M. K. H. Pulok, "Conversion of PSS/E models into RSCAD models: Lessons learned," in *IECON 2014 - 40th Annual Conference of the IEEE Industrial Electronics Society*. Dallas, TX, USA: IEEE, Oct. 2014, pp. 3743–3749.

[17] L. Ljung, *System identification: theory for the user*, 2nd ed., ser. Prentice Hall information and system sciences series. Upper Saddle River, NJ: Prentice Hall PTR, 1999.

[18] A. Phadke and J. Thorp, *Synchronized Phasor Measurements and Their Applications*, ser. Power Electronics and Power Systems. Boston, MA: Springer US, 2008.

[19] J. Bednar and T. Watt, "Alpha-trimmed means and their relationship to median filters," *IEEE Transactions on Acoustics, Speech, and Signal Processing*, vol. 32, no. 1, pp. 145–153, Feb. 1984. [Online]. Available: http://ieeexplore.ieee.org/document/1164279/

[20] A. K. Tangirala, *Principles of system identification: theory and practice*. Boca Raton: CRC Press, Taylor & Francis Group, 2015.

[21] (2016) MATLAB system identification toolbox (r2016a). The Mathworks, Inc. Natick, Massachusetts.

[22] R Core Team. (2018) R: A language and environment for statistical computing. R Foundation for Statistical Computing. Vienna, Austria.

[23] F. Badrkhani Ajaei, "Non-pilot protection of the HVDC grid," Ph.D. dissertation, University of Toronto, Dept. of Electrical and computer engineering, Jun. 2016.

[24] B. Pal and B. Chaudhuri, *Robust control in power systems*. Springer Science & Business Media, 2006.

[25] M. Pai, *Energy function analysis for power system stability*. Springer Science & Business Media, 2012.

[26] P. M. Anderson and A. A. Fouad, *Power system control and stability*, 2nd ed. Wiley-IEEE Press, 2003.

[27] "PSCAD©IEEE 09 bus system," Manitoba Hydro International Ltd., May 2018, accessed: 2020-05-17. [Online]. Available: https://www.pscad.com/knowledge-base/article/25

[28] "PSCAD©IEEE 39 bus system," Manitoba Hydro International Ltd., May 2018, accessed: 2020-05-17. [Online]. Available: https://www.pscad.com/knowledge-base/article/28

[29] *IEEE/IEC Measuring relays and protection equipment Part 24: Common format for transient data exchange (COMTRADE) for power systems*, Std., April 2013.

[30] A. Boratkar, "An improved PMU model for voltage response in transient stability simulation," Master's thesis, Univ. of Toronto, Dept. of Electrical and computer engineering, Nov. 2019.

[31] Grid Protection Alliance, "OpenECA." [Online]. Available: https://github.com/GridProtectionAlliance/openECA

[32] P. F. Velleman and D. C. Hoaglin, *Applications, basics, and computing of explanatory data analysis*. Boston: Duxbury, 1981.

Zhen Dai (S'12–M'19) received the B.E. degree from Tsinghua University, China in 2011, and the Ph.D. degree in electrical engineering at University of Toronto, Canada in 2019.

Joseph Euzebe Tate (S'03–M'08) received the Ph.D. degrees in electrical and computer engineering from the University of Illinois at Urbana-Champaign, Urbana, IL, USA, in 2008. He is currently an Associate Professor at the University of Toronto, Toronto, ON, Canada.